Influence of sub-10 nm anodic alumina nanowire morphology formed by two-step anodizing aluminum on water wettability and slipping behavior

Tatsuya Kikuchi*, Fumiya Onoda, Mana Iwai, Ryosuke O. Suzuki

Faculty of Engineering, Hokkaido University, N13-W8, Kita-ku, Sapporo, Hokkaido, 060-8628, Japan

*Corresponding author: Tatsuya Kikuchi

e-mail: kiku@eng.hokudai.ac.jp

Abstract

The influence of the nanomorphology of alumina nanowires (ANWs) fabricated by a two-step anodizing process on the superhydrophobicity was investigated through advancing contact angle (ACA) and receding contact angle (RCA) measurements. Aluminum nanobowl specimens were anodized in pyrophosphoric acid to fabricate an ordered ANW structure with an average diameter of 7.1 nm, and the outermost surface of the ANWs was chemically bonded with fluorinated self-assembled monolayers. The growing ANWs bent immediately their own weight, and pyramidal ANW structures were formed as they joined the surrounding nanowires together. The ACA value increased with the number density of pyramidal ANW structures due to the reducing area fraction of ANWs, and an increased superhydrophobicity with a contact angle of approximately 165° was measured on the low-density pyramidal structure with a density of 8.1×10^{11} m^{-2}. Additional anodizing led to complete nanowire bending; thus, the advancing contact angle decreased. The pyramidal nanowire structure exhibited a large slipping property with a contact angle hysteresis (CAH) < 10°, whereas the bent nanowire structure exhibited a decreased slipping property with a CAH > 100°. Superhydrophobic surfaces with opposite water slipping properties were demonstrated by a water dropping experiment.

Keywords: Anodizing, Aluminum nanobowls, Alumina nanowires, Contact angle, Superhydrophobicity

1. Introduction

An improvement in the water wettability of industrial aluminum products is one of the key advances needed to improve their self-cleaning properties, heat exchange rate, anti-fog properties, and corrosion protection. Because such wettability greatly depends on the nanoscale and microscale morphologies fabricated on the outermost surface of aluminum products, various surface finishing processes, such as laser irradiation [1-5], coatings [6-9], and plasma electrolytic oxidation (or microarc oxidation) [10,11], have been widely investigated for wettability modification. In particular, an electrochemical passivation process well known as anodizing easily enables the formation of three-dimensional oxide nano- and micron-sized structures [12-20]. Recently, remarkable wettabilities, including superhydrophilicity indicated by a water contact angle lower than 10° and superhydrophobicity indicated by a water contact angle higher than 150°, have been exhibited by micron- and nano-sized structures created on an aluminum surface by anodizing. Because the top surface of the porous oxide film formed by anodizing possesses a unique honeycomb concavo-convex structure, the surface exhibits superhydrophilic and superhydrophobic behaviors [21-23]. In addition, the wettability control on various materials can be achieved via the replication process using the porous oxide film [24-26]. As the porous oxide film is excessively immersed in acidic solutions during or after anodizing, the top surface of the anodic oxide is gradually dissolved into the solution, and alumina nanowires (ANWs), which are different from the typical structures of barrier and porous films, are formed. The aluminum surface covered with these ANWs exhibits higher superhydrophilic and superhydrophobic behaviors [27-33]. These techniques are based on the typical anodizing method using sulfuric, oxalic, and phosphoric acid solutions. However, the nanostructures of ANWs, including their uniformity, length, diameter, and density, could not be accurately controlled via long-term anodizing and chemical etching.

We previously reported the fabrication of superhydrophilic and superhydrophobic aluminum surfaces covered with sub10-nm ANWs by anodizing in pyrophosphoric acid [34-37]. The hydrophilic ANW-covered aluminum surface exhibited a high superhydrophilicity with rapid water evaporation, and we found that the nanostructure consisting of many ANWs strongly affected the superhydrophilic behavior on the surface [38,39]. Conversely, the surface demonstrated a high superhydrophobicity when the ANWs were chemically modified with low surface tension molecules [40,41]. However, the effect of the nanoscale ANWs grown during anodizing on the superhydrophobicity of the aluminum surface is still unsettled in detail; thus, the ANW nanostructures must be precisely controlled during anodizing in pyrophosphoric acid to obtain a deeper understanding of the superhydrophobicity on aluminum surfaces covered with ANWs.

In the current study, we fabricated a superhydrophobic aluminum surface modified precisely with

ANWs via two-step anodizing, and the water wettability and slipping behavior were investigated in detail through advancing and receding contact angle measurements. In contrast to the conventional simple anodizing method, the two-step anodizing process provides higher controllability of the individual ANW structure, such as the length and distance. We revealed the effect of the anodized ANW morphology that consisted of a pyramidal ANW structure on the superhydrophobicity and slipping behavior on the nanostructured surface. Moreover, superhydrophobic surfaces with completely different water sliding properties that were fabricated by precise control of the anodizing time and the corresponding ANW morphology were demonstrated.

2. Experimental methods

Substrates comprising 4N aluminum plates were cleaned ultrasonically in 99.5 wt% ethanol for 10 min and then polished by an electrochemical technique at a constant voltage of 28 V in 22 vol% perchloric acid (70 wt%)/78 vol% acetic acid at 280 K for 1 min. The mirror-polished aluminum specimens were anodized in a 0.3 M oxalic acid solution at 290 K at a constant voltage of 40 V for 120 min using a direct power supply (Kikusui Electronics, PWR400M) to form a porous oxide structure on the aluminum surface (first anodizing). This procedure induced the rearrangement of the bottom porous oxide distribution during the anodizing process, and an ordered honeycomb configuration was fabricated [42]. A platinum plate was employed as the cathode, and the current density was monitored with a digital multimeter during the anodizing process (IWATSU, VOAC7602).

After the first anodizing process, the porous oxide structure was chemically dissolved in a 0.2 M chromic acid/0.51 M phosphoric acid solution to fabricate an ordered nanobowl structure on the aluminum surface. The aluminum nanobowl specimens were anodized in a 74 wt% pyrophosphoric acid solution at 283 K at a constant voltage of 40 V for 240 min to form ordered ANWs on the surface (second anodizing process). After the second anodizing process, the specimens were immersed in a 0.5 mM perfluorooctylphosphonic acid (PFOPA)/ethanol solution at 313 K for 24 h, and the outermost surface of the ANWs was chemically bonded with fluorinated PFOPA self-assembled monolayers (SAMs).

The nanomorphologies of the anodic oxide formed via the first and second anodizing processes were examined by field-emission scanning electron microscopy (SEM, JEOL, JSM6500F). The SEM observations were carried out after the specimens were coated with a thin electroconductive platinum layer. High-resolution images of the ANW structures were obtained by transmission electron microscopy (TEM) and scanning transmission electron microscopy (STEM, FEI, Titan Cubed G2 60-300). Atomic force microscopy (AFM, Hitachi High-Technologies, Nanocute) was also employed to characterize the height and the number density of ANW structures. The wettability was evaluated through advancing

contact angle (ACA) and receding contact angle (RCA) measurements with an ultrapure water droplet using an optical contact angle meter (Kyowa Interface Science, DM-501). The sliding behaviors of the water droplet, which was dropped with a needle and splayed with a micropipette, on the 5°- and 90°-tiled superhydrophobic surfaces, were recorded using a digital video camera.

3. Results and Discussion

Fig. 1a shows the current density-time curves during a) the first anodizing process in oxalic acid and b) the second anodizing process in pyrophosphoric acid at the same constant voltage of 40 V. Typical current density-time curve was obtained by the first anodizing process in oxalic acid. This porous oxide formed by the first anodizing process for 120 min was chemically removed, and then the corresponding aluminum nanobowl surface was observed by SEM (Fig. 1b). A honeycomb structure consisting of numerous nanobowls with an average size of approximately 100 nm was formed on the aluminum surface. After chemical dissolution, the aluminum nanobowl specimen was anodized in pyrophosphoric acid at 40 V and 283 K. We previously reported that the ANWs grew stably during anodizing under this operating condition [35], and the anodizing process provides higher controllability of the ANW morphologies by controlling the anodizing time. The current density gradually decreased with the anodizing time for up to 240 min after the early rapid increase and decrease (Fig. 1a). Compared with the current density-time curve in oxalic acid, the current density obtained in pyrophosphoric acid is considerably smaller than that in oxalic acid. Such low current density is typically measured during anodizing in pyrophosphoric acid under various applied voltages [35], and the growth rate of the anodic oxide is slow. This is may be due to the high viscosity and the low electroconductivity of the concentrated pyrophosphoric acid solution.

The surface of the specimens anodized in pyrophosphoric acid was modified with PFOPA to provide a water-repellent finish. Fig. 2a represents the changes in the advancing contact angle (ACA, red) and the receding contact angle (RCA, blue) with the anodizing time using error bars. Here, the measurements of the ACA and RCA values were performed at five different positions on each aluminum specimen, and the values, then, were averaged without the maximum and minimum values. The ACA value for the aluminum nanobowl surface was 105.6°, which indicated that it possessed slight hydrophobicity. The ACA value rapidly increased to approximately 140° after a short anodizing process for 5 min and gradually increased when the anodizing time increased 20 min. The ACA value then rapidly increased once again when the anodizing time increased from 20-25 min, and superhydrophobicity of the anodized surface was indicted by an ACA that was higher than 150°. The ACA value increased gradually and reached a maximum value of 164.5° after the surface was anodized for 120 min, and then decreased to approximately 155° when the anodizing time increased to 240 min. In summary, the SAM-modified

aluminum surface anodized in pyrophosphoric acid possessed a highly hydrophobic nature, and the hydrophobic behavior can be divided into the following three stages: the initial hydrophobic stage with an ACA of 140-145°, the middle superhydrophobic stage with an ACA of 160-165°, and the latter superhydrophobic stage with an ACA of 155°. The RCA values were substantially changed by increasing the anodizing time. The RCA value measured on the aluminum nanobowl surface was 25.5° and then decreased significantly to 0° when the surface was anodized for 5-10 min. However, the RCA value rapidly increased to approximately 150° when the surface was anodized for 15-25 min and gradually increased to 155° as the anodizing time increased. Finally, the RCA value suddenly dropped to 0° when the surface was anodized for 180 min. The contact angle hysteresis (CAH) is an important parameter of the slipping behavior of a water droplet formed on a surface. The CAH value is defined as the difference between the ACA and PCA values, and the variation of the CAH value as a function of the anodizing time is summarized in Fig. 2b. The early and late stages exhibited a sticky state with high CAH values, whereas the middle stage displayed a slippery state with low CAH values. Compared with the previously reported superhydrophobic surfaces fabricated by the typical anodizing method (ACA values: approximately 150-170°, CAH values: less than 10-70°), similar high superhydrophobicity measuring 150-165° in the ACA value could be achieved via anodizing in pyrophosphoric acid. Moreover, extremely wide CAH values measuring from less than 10° to more than 150° could be obtained by controlling of the anodizing time, thus the slipping and sticking properties of the water droplet on the aluminum surface can be easily controlled by choosing an appropriate anodizing time.

The SEM images of the hydrophobic aluminum specimens formed by the second anodizing process in pyrophosphoric acid are summarized in Fig. 3. When the aluminum nanobowl specimen was anodized for 5 min, a honeycomb porous oxide possessing a periodic nanoscale pore structure was obtained on the surface. Although similar honeycomb oxide structures were also observed on the specimen after anodizing for 10 min, 15 min, and 20 min, the diameter of each pore gradually increased with the anodizing time due to the chemical etching of the aluminum oxide in the pyrophosphoric acid solution. The complete dissolution of the honeycomb oxide structure started after it was anodized for 21 min, and clear convex parts were formed at the triple points of the honeycomb structure. The continued anodizing process enabled the formation and growth of ANWs at the triple points, and the pyramidal ANW structures consisted of several ANWs that appeared on the surface (22 min). The number of ANWs contained in each pyramidal structure gradually increased with anodizing time from 23 min to 30 min due to the growth of the ANWs. Therefore, the size and height of the pyramidal ANW structures increased with anodizing time, and as a result, the number density of the pyramidal structures decreased. Finally, the aluminum surface was covered completely with numerous long ANWs for anodizing times longer

than 180 min.

Based on Figs. 2 and 3, a slippery superhydrophobic surface with higher ACA values and lower CHA values was formed on the aluminum surface covered with pyramidal ANW structures. During advancing and receding contact angle measurements on these surfaces, the water droplet was supported by the top of each hydrophobic pyramidal structure consisting of water-repellent ANWs. To deeply understand the effect of the nanomorphologies on the wettability and slipping behavior, the pyramidal ANW structures were examined by AFM. Fig. 4a shows AFM images of the pyramidal structures formed by the second anodizing process for 22 min, 25 min, and 60 min. Many narrow pyramidal structures were distributed on the whole aluminum surface after 22 min. These pyramidal structures increased in size as the anodizing time increased due to the growth of the ANWs and the joining of surrounding ANWs, and "high ANW mountains" with a low number density were observed on the surface formed after anodizing for 60 min. Figs. 4b and 4c show the changes in the height and the number density of the pyramidal ANW structures with the anodizing time. Here, the average height was measured from the bottom honeycomb structure to the top of the pyramidal structure. The height of the pyramidal structure increased with anodizing time for up to 60 min (from 201 μm for 22 min to 591 μm for 60 min) due to the growth and tangling of the ANWs. However, the height started to decrease after anodizing for more than 80 min, and clear pyramidal structures disappeared from the surface due to the bending of soft amorphous ANWs. Accordingly, the number density of the pyramidal ANW structures drastically decreased with anodizing time (from 3.0×10^{13} m^{-2} for 22 min to 8.1×10^{11} m^{-2} for 100 min).

Fig. 5a represents the effect of the number density of the pyramidal structures, ρ, on the advancing contact angle, and the ACA value increased as the number density decreased. Consequently, an increased superhydrophobic contact angle of approximately 165° was caused by the low-density pyramidal structures. This superhydrophobicity was due to the formation of a composite structure consisting of water/ANW and water/air interfaces, and in this state, the water droplet did not penetrate into the concave parts of the composite structure (Cassie-Baxter state) [43]. Cassie and Baxter developed an equation for the steady-state contact angle on the composite structure as follows [44]:

$$\cos\theta_{CA} = f_1 \cos\theta_1 + f_2 \cos\theta_2 \qquad (1)$$

where θ_{CA} is the contact angle; f_1 and f_2 are the area fractions of the solid and the air at the interface, respectively; and θ_1 and θ_2 are the contact angles measured on the flat solid and air surfaces, respectively. Then, equation (1) becomes:

$$\cos\theta_{CA} = f_1 \cos\theta_1 + (1 - f_1) \cos\theta_2 \qquad (2)$$

Here, equation (2) can be rewritten when $\theta_2 = 180°$ as:

$$\cos\theta_{CA} = f_1 \cos\theta_1 + f_1 - 1 \qquad (3)$$

The relationship between the calculated contact angle and the area fraction of solid at the composite interface in the Cassie-Baxter state is shown in Fig. 5b. The calculated contact angle gradually increased as the area fraction of solid decreased, and a similar curved relation between the experimental result and the Cassie-Baxter model was obtained. The maximum ACA value obtained experimentally remained at approximately 165° on the surface that contained the minimum number density of the pyramidal structures (Fig. 5a), and additional low-density pyramidal structures may result in an increased superhydrophobic contact angle of more than 165°. However, the amorphous ANWs formed by long-term anodizing were completely bent due to their own weight; thus, the pyramidal structures were not present on the surface (Fig. 3). Therefore, there may be a limitation to increasing the superhydrophobicity by decreasing the number density of the pyramidal structures formed by anodizing in pyrophosphoric acid.

As the shape of the contact area on each of the pyramidal structures that supported the water droplet was assumed to be a circle, the real area fraction of the pyramidal structures, $f_{1\text{-real}}$, can be calculated as follows:

$$f_{1\text{-real}} = \rho\pi r^2 \qquad (4)$$

where r is the radius of each circular contact area. The number density of the pyramidal structures formed after anodizing for 22 min was 2.98×10^{13} m^{-2} (Fig. 3), and the ACA value was measured to be approximately 152° (Figs. 2a and 5a). The value of r that satisfied these experimental results was calculated to be approximately 50 nm using equation (4). Fig. 6 shows a) a bright-field (BF) STEM image and b) a high-resolution TEM image of the pyramidal ANW structures formed by anodizing for 22 min. A porous oxide structure measuring approximately 100 nm in thickness was formed on the aluminum substrate, and pyramidal structures consisting of sub10-nm scale ANWs formed by the chemical dissolution of aluminum oxide were observed on the porous oxide. We previously found that the ANWs grew and become longer with the anodizing time, whereas the thickness of the porous layer was almost unchanged due to the rapid dissolution of pore walls [35]. Therefore, only the ANWs grows longer length during anodizing. The average diameter of the ANWs was measured to be 7.1 nm. Although the size of the outermost part of the pyramidal structures increased due to the bundling of multiple ANWs, their width was measured to be approximately 10-15 nm, which differed from the calculated value (50 nm). Therefore, the shape of the pyramidal structures was expected to be quite pressed and transformed by the weight of the supported water droplet during the contact angle investigations.

We demonstrated the slipping behavior of a water droplet on the superhydrophobic surfaces with low CAH values that were produced by the long ANW structures and high CAH values that were produced by the pyramidal ANW structures. Fig. 7 shows video snapshots of the sliding behavior of a water droplet on the 5°-tilted superhydrophobic specimens. Here, a 12.5 μL water droplet was

continuously dropped on the superhydrophobic surface from a needle. When a water droplet was dropped onto the long ANW structures (Fig. 7a), the droplet became stuck on the nanostructured surface and did not slip. Although the size of the water droplet increased due to a continuous water supply and the shape gradually changed to an ellipsoid, the large droplet also became stuck to the surface. In contrast, as the water droplet was applied to the pyramidal ANW structures (Fig. 7b), the droplet immediately slipped down to the right side without any sticking.

These superhydrophobic specimens with different CAH values were vertically placed on a laboratory table, and a 10 μL water droplet was splayed toward the specimen using a micropipette (Fig. 8). In the case of the long ANW structures (Fig. 8a), the water droplet released from the pipette became stuck on the 90°-tiled superhydrophobic surface without any splashing due to their low CAH value. Such sticking behavior occurred on the whole anodized surface (right, Fig. 8a). Conversely, the water droplet applied to the pyramidal ANW structures was dispersed everywhere and did not stick due to the high CAH value, and the surface remained clean (Fig. 8b). Based on Figs. 7 and 8, even though similar superhydrophobic aluminum surfaces were covered with ANWs, completely different slipping behaviors were easily obtained by controlling the anodizing time and the corresponding CAH value.

4. Conclusions

We investigated the influence of the ANW morphology, including a pyramidal ANW structure, on the water wettability and slipping behavior on a hydrophobic surface fabricated via a two-step aluminum anodizing process. The ANWs immediately formed pyramidal ANW structures during the early stage of anodizing, and their pyramidal structures increased in size due to joining of the surrounding nanowires. The advancing contact angle increased with the number density of pyramidal ANW structures due to a reducing area fraction of the solid/liquid interface, and a highest superhydrophobic contact angle measuring approximately 165° was obtained on a low-density pyramidal structure with a density of 8.1×10^{11} m^{-2}. Further anodizing led to complete nanowire bending and the disappearance of the pyramidal structures due to the growth of long ANWs; thus, the advancing contact angle decreased. The pyramidal ANW structure exhibited high slipping value indicated by a CAH < 10°, whereas the bent nanowire structure exhibited a lower slipping value indicated by a CAH > 100°. Superhydrophobic surfaces with a range of water slipping properties can be fabricated by controlling the anodizing time and the corresponding CAH value.

Acknowledgments

This work was supported by the Japan Society for the Promotion of Science, KAKENHI (grant

number: 19H02470) in addition to the Amano Industrial Technology Laboratory, and Nanotechnology Platform Program of the Ministry of Education, Culture, Sports, Science and Technology (grant numbers: A-19-HK-0034 and A-20-HK-0037). The authors thank Mr. Nobuyuki Miyazaki, Dr. Takashi Endo, and Mr. Ryo Oota for their technical assistance.

References

1) C. V. Ngo, D. M. Chun, Control of laser-ablated aluminum surface wettability to superhydrophobic or superhydrophilic through simple heat treatment or water boiling post-processing, Appl. Surf. Sci., 435 (2018) 974-982. https://doi.org/10.1016/j.apsusc.2017.11.185

2) S. Milles, B. Voisiat, M. Nitschke, A. F. Lasagni, Influence of roughness achieved by periodic structures on the wettability of aluminum using direct laser writing and direct laser interference patterning technology, J. Mater. Process. Technol., 270 (2019) 142-151. https://doi.org/10.1016/j.jmatprotec.2019.02.023

3) W. Liu, M. Cai, X. Luo, C. Chen, R. Pan, H. Zhang, M. Zhong, Wettability transition modes of aluminum surfaces with various micro/nanostructures produced by a femtosecond laser, J. Laser Appl., 31 (2019) 022503. https://doi.org/10.2351/1.5096076

4) J. Li, Y. Zhou, F. Fan, F. Du H. Yu, Controlling surface wettability and adhesive properties by laser marking approach, Opt. Laser Technol., 115 (2019) 160-165. https://doi.org/10.1016/j.optlastec.2019.02.023

5) Y. Qin, Y. Li, D. Zhang, N. Xu X. Zhu, Wettability, durability and corrosion properties of slippery laser-textured aluminum alloy surface under water impact, Surf. Coat. Technol., 394 (2020) 125856. https://doi.org/10.1016/j.surfcoat.2020.125856

6) L. Yin, Y. Wang, J. Ding, Q. Wang Q. Chen, Water condensation on superhydrophobic aluminum surfaces with different low-surface-energy coatings, Appl. Surf. Sci., 258 (2012) 4063-4068. https://doi.org/10.1016/j.apsusc.2011.12.100

7) T. J. Young, J. Jackson, S. Roy, H. Ceylan, S. Sundararajan, Tribological behavior and wettability of spray-coated superhydrophobic coatings on aluminum, Wear, 376, (2017) 1713-1719. https://doi.org/10.1016/j.wear.2016.12.050

8) J. Xiong, D. K. Sarkar, X. G. Chen, Superhydrophobic honeycomb-like cobalt stearate thin films on aluminum with excellent anti-corrosion properties, Appl. Surf. Sci., 407 (2017) 361-370. https://doi.org/10.1016/j.apsusc.2017.02.203

9) H. Yang, Y. He, Z. Wu, J. Miao, F. Yang, Z. Lu, Fabrication of a superhydrophobic and high-glossy copper coating on aluminum substrates, Appl. Surf. Sci., 433 (2018) 1192-1196.

https://doi.org/10.1016/j.apsusc.2017.10.130

10) S. V. Gnedenkov, S. L. Sinebryukhov, V. S. Egorkin, I. E. Vyaliy, Wettability and electrochemical properties of the highly hydrophobic coatings on PEO-pretreated aluminum alloy Surf. Coat. Technol., 307 (2016) 1241-1248. https://doi.org/10.1016/j.surfcoat.2016.07.074

11) L. Pezzato, M. Rigon, A. Martucci, K. Brunelli, M. Dabalà, Plasma Electrolytic Oxidation (PEO) as pre-treatment for sol-gel coating on aluminum and magnesium alloys Surf. Coat. Technol., 366 (2019) 114-123. https://doi.org/10.1016/j.surfcoat.2019.03.023

12) H. Masuda, K. Fukuda, Ordered metal nanohole arrays made by a two-step replication of honeycomb structures of anodic alumina, Science, 268 (1995) 1466-1468. https://doi.org/10.1126/science.268.5216.1466

13) W. Lee, S. J. Park, Porous anodic aluminum oxide: anodization and templated synthesis of functional nanostructures, Chem. Rev., 114 (2014) 7487-7556. https://doi.org/10.1021/cr500002z

14) L. Wen, R. Xu, Y. Mi, Y. Lei, Multiple nanostructures based on anodized aluminium oxide templates, Nat. Nanotechnol., 12 (2017) 244-250. https://doi.org/10.1038/nnano.2016.257

15) H. Asoh, K. Nishio, M. Nakao, T. Tamamura, H. Masuda, Conditions for fabrication of ideally ordered anodic porous alumina using pretextured Al, J. Electrochem. Soc., 148 (2001) B152-B156. https://doi.org/10.1149/1.1355686

16) H. Asoh, S. Ono, T. Hirose, M. Nakao, H. Masuda, Growth of anodic porous alumina with square cells, Electrochim. Acta, 48 (2003) 3171-3174. https://doi.org/10.1016/S0013-4686(03)00347-5

17) G. D. Sulka, K. Hnida, Distributed Bragg reflector based on porous anodic alumina fabricated by pulse anodization, Nanotechnology, 23 (2012) 075303. https://doi.org/10.1088/0957-4484/23/7/075303

18) G. D. Sulka, W. J. Stępniowski, Structural features of self-organized nanopore arrays formed by anodization of aluminum in oxalic acid at relatively high temperatures, Electrochim. Acta, 54 (2009) 3683-3691. https://doi.org/10.1016/j.electacta.2009.01.046

19) S. Akiya, T. Kikuchi, S. Natsui, R. O. Suzuki, Nanostructural characterization of large-scale porous alumina fabricated via anodizing in arsenic acid solution, Appl. Surf. Sci. 403 (2017) 652- 661. https://doi.org/10.1016/j.apsusc.2017.01.243

20) M. Iwai, T. Kikuchi, R. O. Suzuki, Initial structural changes of porous alumina film via high-resolution microscopy observations, ECS J. Solid State Sci. Technol. 9 (2020) 044004. https://doi.org/10.1149/2162-8777/ab89ba

21) W. Lee, B. G. Park, D. H. Kim, D. J. Ahn, Y. Park, S. H. Lee, K. B. Lee, Nanostructure-dependent water-droplet adhesiveness change in superhydrophobic anodic aluminum oxide surfaces: from highly

adhesive to self-cleanable, Langmuir 26 (2010) 1412-1415. https://doi.org/10.1021/la904095x

22) J. G. Buijnsters, R. Zhong, N. Tsyntsaru, J. P. Celis, Surface wettability of macroporous anodized aluminum oxide, ACS Appl. Mater. Interfaces. 5 (2013) 3224-3233. https://doi.org/10.1021/am4001425

23) J. Zang, S. Yu, G. Zhu, X. Zhou, Fabrication of superhydrophobic surface on aluminum alloy 6061 by a facile and effective anodic oxidation method, Surf. Coat. Technol., 380, (2019) 125078. https://doi.org/10.1016/j.surfcoat.2019.125078

24) K. Lee, S. Lyu, S. Lee, Y. S. Kim, W. Hwang, Characteristics and self-cleaning effect of the transparent super-hydrophobic film having nanofibers array structures, Appl. Surf. Sci., 256 (2010) 6729-6735. https://doi.org/10.1016/j.apsusc.2010.04.081

25) J. H. Kong, T. H. Kim, J. H. Kim, J. K. Park, D. W. Lee, S. H. Kim, J. M. Kim, Highly flexible, transparent and self-cleanable superhydrophobic films prepared by a facile and scalable nanopyramid formation technique, Nanoscale, 6, (2014) 1453-1461. https://doi.org/10.1039/C3NR04629J

26) T. Yanagishita, K. Murakoshi, T. Kondo, H. Masuda, Preparation of superhydrophobic surfaces with micro/nano alumina molds, RSC. Adv. 8 (2018) 36697-36704. https://doi.org/10.1039/C8RA07497F

27) W. Wu, X. Wang, D. Wang, M. Chen, F. Zhou, W. Liu, Q. Xue, Alumina nanowire forests via unconventional anodization and super-repellency plus low adhesion to diverse liquids, Chem. Commun., 9 (2009) 1043-1045. https://doi.org/10.1039/B818633B

28) B. G. Park, W. Lee, J. S. Kim, K. B. Lee, Superhydrophobic fabrication of anodic aluminum oxide with durable and pitch-controlled nanostructure, Colloid Surf. A: Physicochem. Eng. Asp. 370 (2010) 15-19. https://doi.org/10.1016/j.colsurfa.2010.08.014

29) C. Jeong, C. H. Choi, Single-step direct fabrication of pillar-on-pore hybrid nanostructures in anodizing aluminum for superior superhydrophobic efficiency, ACS Appl. Mater. Inter., 4, (2012) 842-748. https://doi.org/10.1021/am201514n

30) S. Peng, D. Tian, X. Yang, W. Deng, Highly efficient and large-scale fabrication of superhydrophobic alumina surface with strong stability based on self-congregated alumina nanowires, ACS Appl. Mater. Inter., 6, (2014) 4831-4841. https://doi.org/10.1021/am4057858

31) H. Saffari, B. Sohrabi, M. R. Noori, H. R. T. Bahrami, Optimal condition for fabricating superhydrophobic aluminum surfaces with controlled anodizing processes, Appl. Surf. Sci., 435 (2018) 1322-1328. https://doi.org/10.1016/j.apsusc.2017.11.188

32) S. Y. Li, X. G. Xiang, B. H. Ma, X. D. Meng, Facile preparation of diverse alumina surface structures by anodization and superhydrophobic surfaces with tunable water droplet adhesion, J. Alloys Compd., 779 (2019) 219-228. https://doi.org/10.1016/j.jallcom.2018.11.222

33) C. Jeong, H. Ji, Systematic control of anodic aluminum oxide nanostructures for enhancing the superhydrophobicity of 5052 aluminum alloy, Materials, 12 (2019) 3231. https://doi.org/10.3390/ma12193231

34) T. Kikuchi, O. Nishinaga, D. Nakajima, J. Kawashima, S. Natsui, N. Sakaguchi, R. O. Suzuki, Ultra-high density single nanometer-scale anodic alumina nanofibers fabricated by pyrophosphoric acid anodizing, Sci. Rep., 4 (2014) 1-6. https://doi.org/10.1038/srep07411

35) D. Nakajima, T. Kikuchi, S. Natsui, N. Sakaguchi, R. O. Suzuki, Fabrication of a novel aluminum surface covered by numerous high-aspect-ratio anodic alumina nanofibers, Appl. Surf. Sci., 356 (2015) 54-62. https://doi.org/10.1016/j.apsusc.2015.08.030

36) R. Kondo, D. Nakajima, T. Kikuchi, S. Natsui, R. O. Suzuki, Superhydrophilic and superhydrophobic aluminum alloys fabricated via pyrophosphoric acid anodizing and fluorinated SAM modification, J. Alloys Compd., 725 (2017) 379-387. https://doi.org/10.1016/j.jallcom.2017.07.183

37) D. Nakajima, T. Kikuchi, S. Natsui, R. O. Suzuki, Highly ordered anodic alumina nanofibers fabricated via two distinct anodizing processes, ECS Electrochem. Lett., 4 (2015) H14-H17. https://doi.org/10.1149/2.0021505eel

38) D. Nakajima, T. Kikuchi, S. Natsui, R. O. Suzuki, Superhydrophilicity of a nanofiber-covered aluminum surface fabricated via pyrophosphoric acid anodizing, Appl. Surf. Sci., 389 (2016) 173-180. https://doi.org/10.1016/j.apsusc.2016.06.088

39) D. Nakajima, T. Kikuchi, T. Yoshioka, H. Matsushima, M. Ueda, R. O. Suzuki, S. Natsui, A superhydrophilic aluminum surface with fast water evaporation based on anodic alumina bundle structures via anodizing in pyrophosphoric acid, Materials, 12 (2019) 3497. https://doi.org/10.3390/ma12213497

40) D. Nakajima, T. Kikuchi, S. Natsui, R. O. Suzuki, Mirror-finished superhydrophobic aluminum surfaces modified by anodic alumina nanofibers and self-assembled monolayers., Appl. Surf. Sci., 440 (2018) 506-513. https://doi.org/10.1016/j.apsusc.2018.01.182

41) D. Nakajima, T. Kikuchi, S. Natsui, R. O. Suzuki, Advancing and receding contact angle investigations for highly sticky and slippery aluminum surfaces fabricated from nanostructured anodic oxide, RSC Adv., 8 (2018) 37315-37323. 10.1039/C8RA07712F

42) H. Ikeda, M. Iwai, D. Nakajima, T. Kikuchi, S. Natsui, N. Sakaguchi, R. O. Suzuki, Nanostructural characterization of ordered gold particle arrays fabricated via aluminum anodizing, sputter coating, and dewetting, Appl. Surf. Sci., 465 (2019) 747-753. https://doi.org/10.1016/j.apsusc.2018.09.229

43) A. Giacomello, S. Meloni, M. Chinappi, C. M. Casciola, Cassie–Baxter and Wenzel states on a

nanostructured surface: phase diagram, metastabilities, and transition mechanism by atomistic free energy calculations, Langmuir, 28 (2012) 10764-10772. https://doi.org/10.1021/la3018453

44) H. Y. Erbil, C. E. Cansoy, Range of applicability of the Wenzel and Cassie− Baxter equations for superhydrophobic surfaces, Langmuir, 25 (2009) 14135-14145. https://doi.org/10.1021/la902098a

Figure Captions

Figure 1 a) Current density-time curves during aluminum anodizing at a constant voltage of 40 V in a 0.3 M oxalic acid solution at 290 K (first anodizing process) and a 74 wt% pyrophosphoric acid solution at 283 K (second anodizing process). b) SEM image of the aluminum nanobowl surface fabricated by anodizing in oxalic acid and subsequent oxide removal.

Figure 2 a) Changes in the advancing contact angle (ACA) and the receding contact angle (RCA) of a water droplet with anodizing time during second anodizing in pyrophosphoric acid. b) The change in the contact angle hysteresis (CAH) with the anodizing time.

Figure 3 SEM images of the anodized aluminum surface in a 74 wt% pyrophosphoric acid solution at 283 K from 5 min to 180 min.

Figure 4 a) AFM images of the pyramidal alumina nanowire (ANW) structures formed by anodizing for 22 min, 25 min, and 60 min. b) The change in the height of pyramidal structures with the anodizing time. c) The change in the number density of pyramidal structures with anodizing time.

Figure 5 a) The relationship between the advancing contact angle and the number density of pyramidal structures. b) The change in the calculated contact angle with the area fraction of solid at the interface of the Cassie-Baxter state.

Figure 6 a) A BF-SETM image and b) high-resolution TEM image of the pyramidal ANW structure fabricated by the second anodizing process for 22 min.

Figure 7 Video snapshots of a 12.5 μL water droplet dropped from a needle onto the 5°-tilted superhydrophobic surfaces with a) a high CAH value and b) a low CAH value.

Figure 8 Video snapshots of a 10 μL water droplet splayed from a micropipette onto 90°-tiled superhydrophobic surfaces with a) a high CAH value and b) a low CAH value.

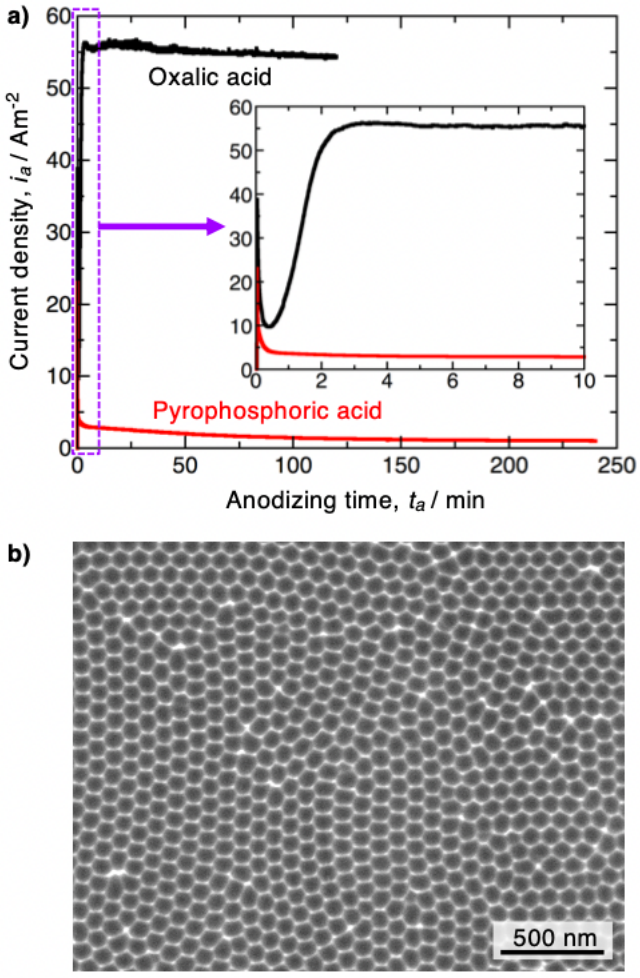
a)
Oxalic acid
Pyrophosphoric acid
Current density, i_a / Am^{-2}
Anodizing time, t_a / min
b)
500 nm

Figure 1.

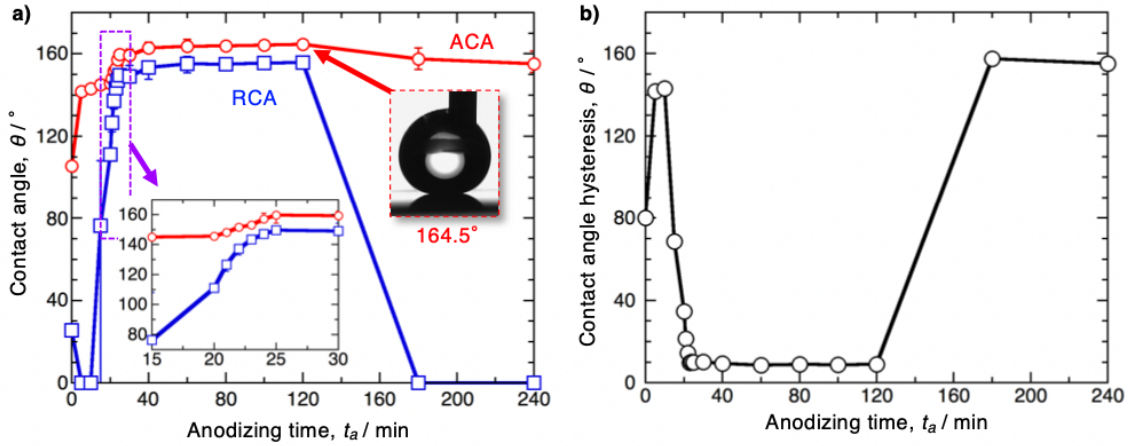
a)
b)
ACA
RCA
164.5°
Contact angle, θ / °
Anodizing time, t_a / min
Contact angle hysteresis, θ / °
Anodizing time, t_a / min

Figure 2.

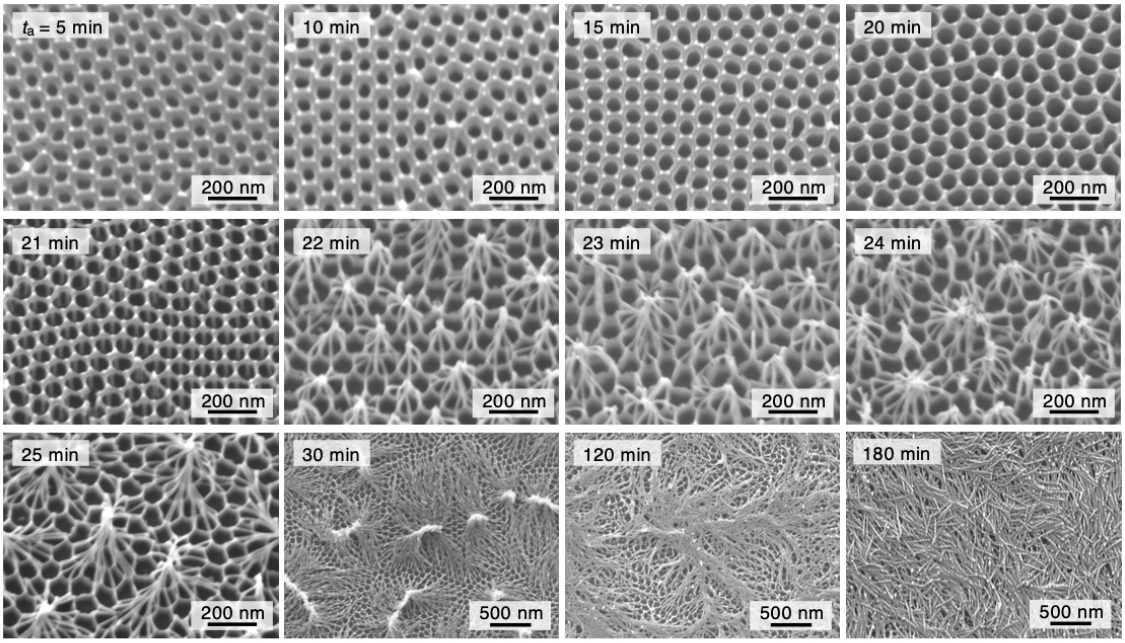
t_a = 5 min
200 nm
10 min
200 nm
15 min
200 nm
20 min
200 nm
21 min
200 nm
22 min
200 nm
23 min
200 nm
24 min
200 nm
25 min
200 nm
30 min
500 nm
120 min
500 nm
180 min
500 nm

Figure 3.

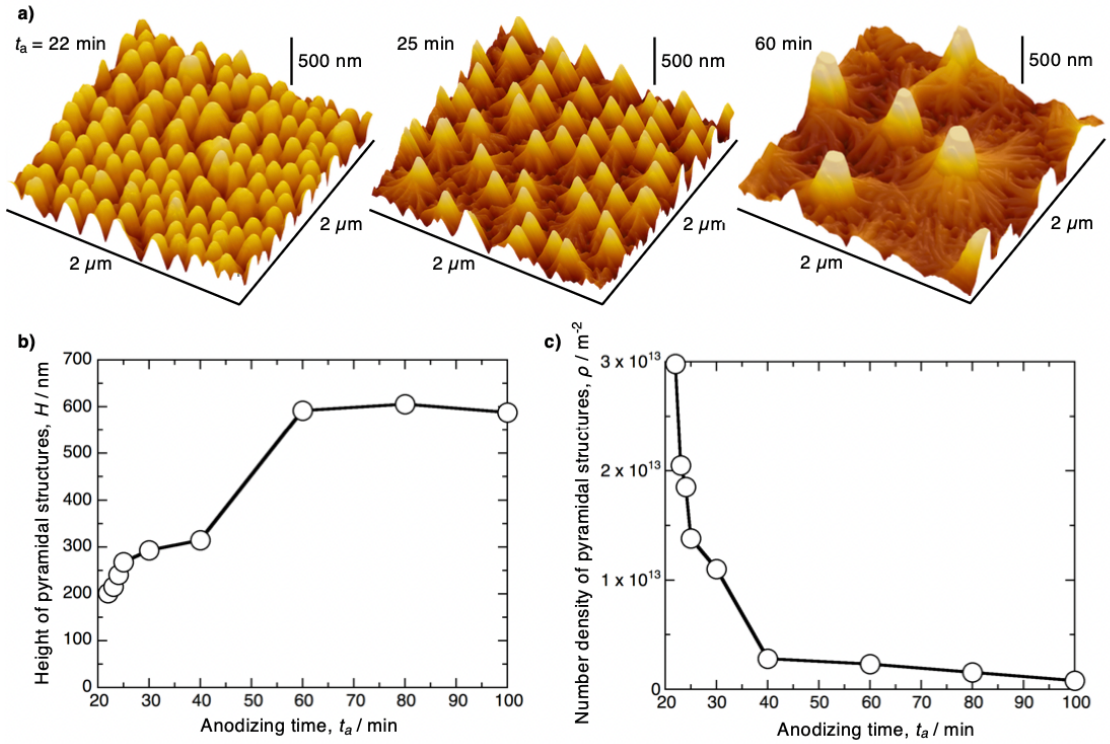
a)
t_a = 22 min
500 nm
2 μm
2 μm
25 min
500 nm
2 μm
2 μm
60 min
500 nm
2 μm
2 μm
b)
Height of pyramidal structures, H / nm
700
600
500
400
300
200
100
0
20
30
40
50
60
70
80
90
100
Anodizing time, t_a / min
c)
Number density of pyramidal structures, ρ / m^{-2}
3 x 10^{13}
2 x 10^{13}
1 x 10^{13}
0
20
30
40
50
60
70
80
90
100
Anodizing time, t_a / min

Figure 4.

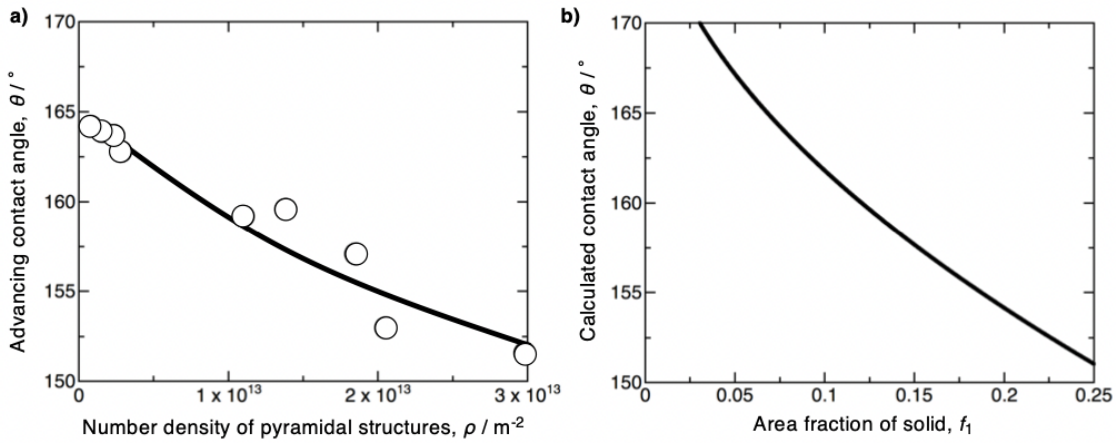
a)
170
165
160
155
150
Advancing contact angle, θ / °
0
1 x 10^13
2 x 10^13
3 x 10^13
Number density of pyramidal structures, ρ / m^-2
b)
170
165
160
155
150
Calculated contact angle, θ / °
0
0.05
0.1
0.15
0.2
0.25
Area fraction of solid, f1

Figure 5.

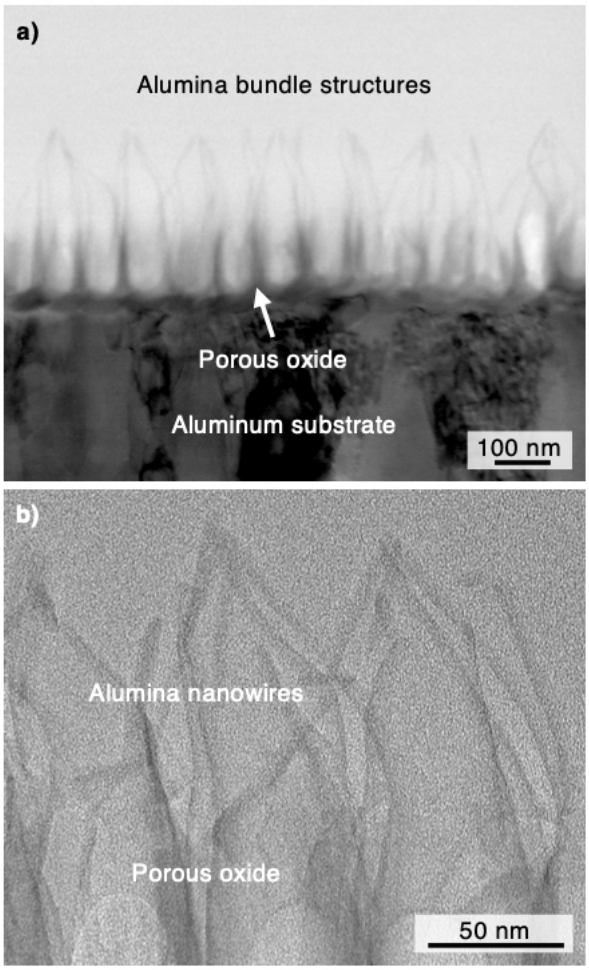
a)
Alumina bundle structures
Porous oxide
Aluminum substrate
100 nm
b)
Alumina nanowires
Porous oxide
50 nm

Figure 6.

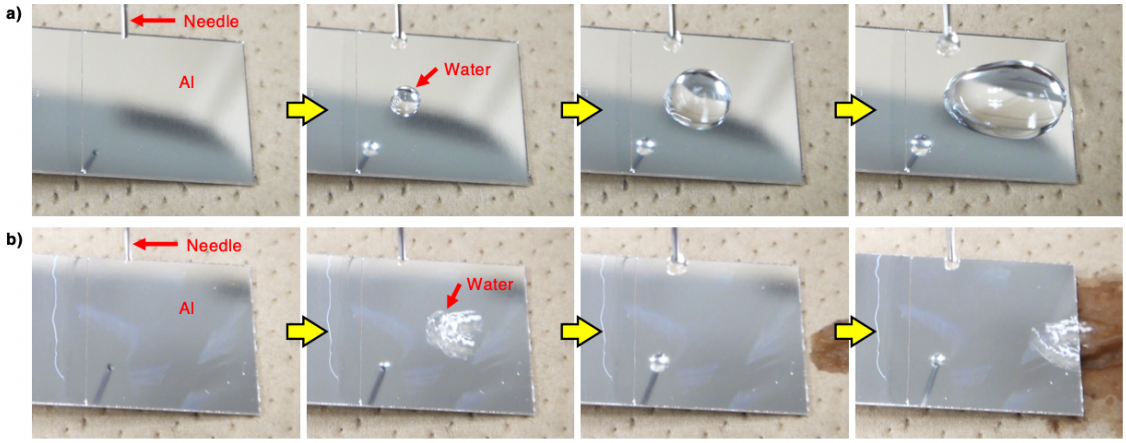

Figure 7.

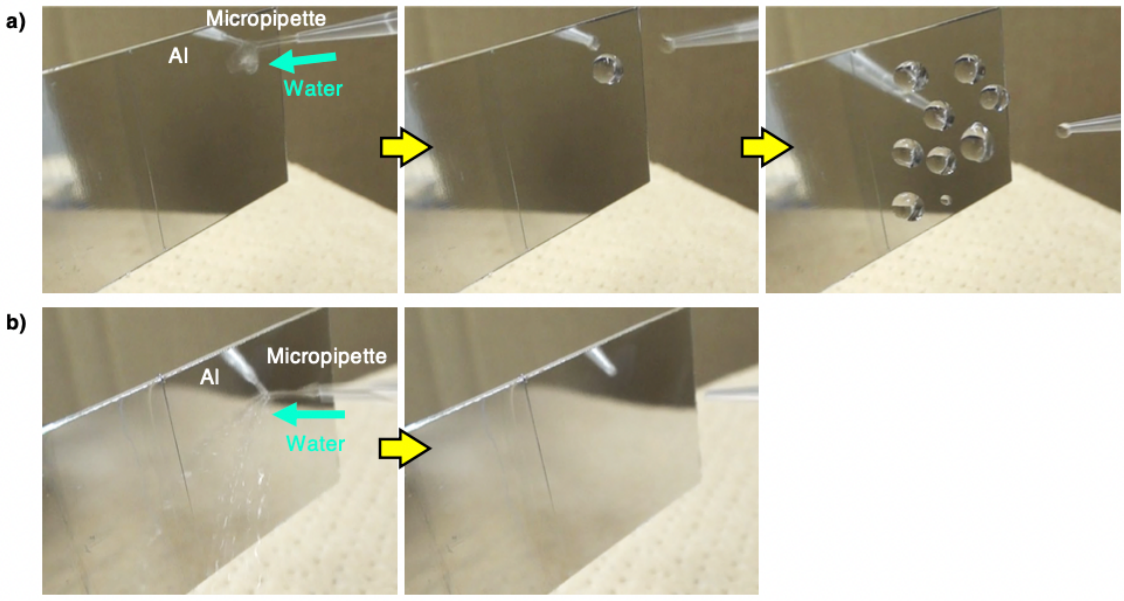

Figure 8.